Upconversion time microscope demonstrating 103× magnification of femtosecond waveforms

C. V. Bennett

Department of Electrical Engineering, University of California, Los Angeles, and Lawrence Livermore National Laboratory, P.O. Box 808, L-174, Livermore, California 94551

B. H. Kolner

Department of Applied Science, 228 Walker Hall, University of California, Davis, Davis, California 95616

Received December 23, 1998

We present the operational principles and results of a temporal imaging system, configured as a time microscope, that achieves 103× magnification of waveforms with 300-fs resolution and a 5.7-ps field of view. The quadratic-phase time-lens element is realized by upconversion of the dispersed input waveform with a linearly chirped 5-THz bandwidth pump. The system allows expansion of ultrafast optical waveforms to a time scale that is directly accessible with slower conventional technology, in real time, on a single-shot basis.

OCIS codes: 320.7100, 320.2250, 320.7160, 190.2620.

Modern approaches to measuring ultrashort optical waveforms invariably suffer from limitations, most notably the requirements of repetitive waveform capture and signal-processing time. The characterization of single transient phenomena or rapidly changing waveform structure necessitates a new approach. In this Letter we describe a temporal imaging system that creates expanded replicas of ultrafast optical waveforms in real time so that they can be recorded with slower conventional technology. The system is, in effect, a microscope operating in the time domain.

Temporal imaging is based on the mathematical analogy between paraxial diffraction and narrow-band dispersion.[1–5] These phenomena introduce quadratic phases into their respective frequency domains, k_x, k_y (transverse wave numbers), and ω (temporal frequency). In both cases these phases are acquired during propagation, scaling as d/k for diffraction and $\xi\beta'' = \phi''$ for dispersion, where d and ξ are propagation distances in a fixed and a traveling-wave coordinate system, respectively, $k = 2\pi/\lambda$ is the wave number in the material, and β'' is the group-velocity dispersion.

A conventional lens imparts a quadratic spatial phase that is proportional to k/f, where the focal length f is a measure of the diffraction required for removal of the phase imparted by the lens. Similarly, one can create a time lens by imparting a quadratic temporal phase (linear frequency chirp $\mathrm{d}\omega/\mathrm{d}\tau$) to a waveform. A temporal focal distance ξ_f or focal group-delay dispersion (GDD), $\phi_f'' = \xi_f\beta'' = -(\mathrm{d}\omega/\mathrm{d}\tau)^{-1}$, is defined as the GDD required for removal of the quadratic phase imparted by the time lens. A temporal imaging system is created by cascading an input GDD (ϕ_1''), a time lens, and an output GDD (ϕ_2'') in proper measure to satisfy the temporal imaging condition

$$1/\phi_1'' + 1/\phi_2'' = 1/\phi_f''. \tag{1}$$

A waveform of arbitrary shape passing through this system emerges temporally rescaled with magnification

$$M = -\phi_2''/\phi_1''. \tag{2}$$

We can facilitate an understanding of this process by drawing temporal ray diagrams,[6] as shown in Fig. 1. The horizontal axis is the propagation distance in units of real distance or accumulated GDD. The vertical axis is local time relative to the group delay. Rays with different slopes in Fig. 1 depict different spectral components $(\omega - \omega_0)$ of the input signal. Unlike diffraction, which has only one sign, GDD (ϕ'') can be positive or negative. This allows two possible single-lens imaging configurations that have either positive or negative magnification. For $M < 0$, all GDD's must be of the same sign, and the diagram looks like its spatial conterpart. For $M > 0$, the output GDD (ϕ_2'') must have the opposite sign of the input and the focal GDD's, analogous to virtual imaging systems in space. Figure 1 shows two pulses at the same carrier frequency being magnified in a system with $M = +3$. The pulses spread as they propagate through the input GDD. The phase-modulation process in the time lens frequency shifts each spectral component (ray), causing

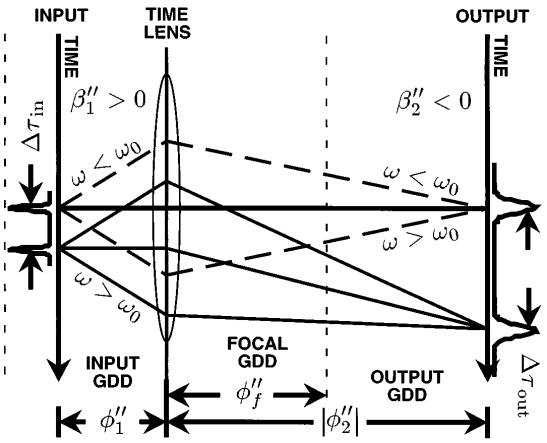

Fig. 1. Temporal ray diagram of a two-pulse sequence with ϕ_1'', $\phi_f'' > 0$, $\phi_2'' < 0$, and $M = +3$. Physical propagation distance ξ is increasing from left to right.

0146-9592/99/110783-03$15.00/0

them to appear bent. The output GDD then focuses the rays, creating a temporally scaled image.

The resolution of a temporal imaging system depends on the bandwidth Δf imparted by the time-lens modulation process and is given approximately by $\delta\tau_{\text{in}} \approx 1/\Delta f$.[4] Any process that imparts a large-bandwidth linear chirp is attractive as a time-lens mechanism. The first optical time lenses used electro-optic phase modulation and demonstrated pulse compression,[7–13] temporal imaging,[14] and time-to-frequency conversion.[15] Many technological challenges limit further improvement of the bandwidth generated with this technique and thus limit its utility. In contrast, the desired bandwidth is already available from current laser sources, providing the motivation for our upconversion temporal imaging approach[16] and a related time-to-frequency conversion technique.[17] In this experiment we utilize the broad bandwidth and easily chirped femtosecond pulses from a Ti:sapphire laser to sum with our input signal in a nonlinear crystal to achieve the required time-lens action. Additionally, the finite duration of the pump acts as a shutter, since no sum-frequency signal appears in the absence of the pump. This is also the dominant factor determining the field of view.

A schematic diagram of our upconversion time microscope is shown in Fig. 2. It was designed for a magnification $M = +100$ and a field of view of $\approx$5 ps. A Ti:sapphire laser producing 87-fs (5.0-THz) pulses at $\lambda = 830$ nm was used as the source for both the time-lens pump and the input test pattern. A two-pulse input test pattern with adjustable delay $\Delta\tau_{\text{in}}$ was created in a Michelson interferometer with a minimum step size of 0.67 fs. We produced the time lens by dispersing a pulse in a folded multipass grating-pair dispersive delay line[18] and mixing it with the dispersed input signal by noncollinear sum-frequency generation in a 500-μm-thick beta barium borate crystal. This pump pulse produced a time lens with an $f\# \equiv \omega_0/\Delta\omega = 82$.[19] The input and output GDD's were also realized with folded multipass grating-pair dispersive delay lines, although lenses were used in the input to change the signal of the GDD.[18,20] Both the input and pump dispersions used 600-groove/mm gratings. The dispersions were characterized by use of spectrally resolved upconversion[21] and resulted in $\phi_1'' = +0.17606$ ps^2 and a time lens with focal GDD $\phi_f'' = +0.17784$ ps^2. The output GDD used a 3600-groove/mm grating and was configured for $\phi_2'' = -17.606$ ps^2.

Figure 3 shows a series of temporal images from the time microscope recorded with a 40-GHz photodiode and sampling oscilloscope. Beginning with the button trace, each successive trace is taken with an additional 667-fs delay of pulse #2 with respect to stationary pulse #1 in the test-pattern generator. The right vertical axis shows the input delay of pulse #2. The bottom axis is the actual photodiode signal time scale. A linear fit to the output versus input time of pulse #2 gives a magnification $M = +103$ with a deviation of 22 fs rms, referred to the input. The top axis is an equivalent input time scale created by division of the output time by the measured magnification. We also recorded images in 100-fs delay steps near $\Delta\tau_{\text{in}} = 0$ fs. For delays as short as $\Delta\tau_{\text{in}} = 300$ fs two pulses were still clearly resolved in the temporal image. When the delay was shorter, interference effects obscured the envelope profiles.

The output spectrum for each temporal image is shown in Fig. 4. This figure demonstrates a very interesting analogy with spatial beam forming. When a diffraction-limited beam enters a lens parallel to the lens axis, the exit angle depends on the displacement of the input beam from the axis. The output beam acquires a new mean spatial frequency corresponding to this exit angle. In our time microscope the input pulses are transform limited and enter the time lens at various delays with respect to the chirp profile. Thus, they acquire a new mean frequency when they exit the time lens, depending on the portion of the chirped pump frequency with which they sum. This is entirely analogous to the spatial case described above and is made apparent in Fig. 4.

In a high-magnification system with an input bandwidth comparable with that of the time lens, the field of view is approximately the duration of the lens. The expected roll-off in the field of view is not readily apparent in Fig. 3. This roll-off could be masked by slight mechanical instabilities affecting the coupling into the photodiode. A more pronounced roll-off can be seen in the spectral data of Fig. 4, which were acquired with a different photodetector. A Gaussian fit to the peak spectral intensity of pulse #2 as a function of input delay gives an input temporal field of view of 5.65 ps FWHM, in good agreement with width of the chirped time-lens pump pulse.

Deviations from ideal quadratic phase in both the dispersion's frequency dependence and the time lens's time dependence cause aberrations. We have discovered that the dominant result of higher-order spectral phase in the input dispersion is to distort the shape of the system's impulse response, whereas in the output dispersion it alters the arrival time of the impulse response. Time-lens aberrations can produce a variety of effects, including analogs to coma and spherical aberration in spatial systems. Phase matching in the nonlinear crystal is required for good conversion

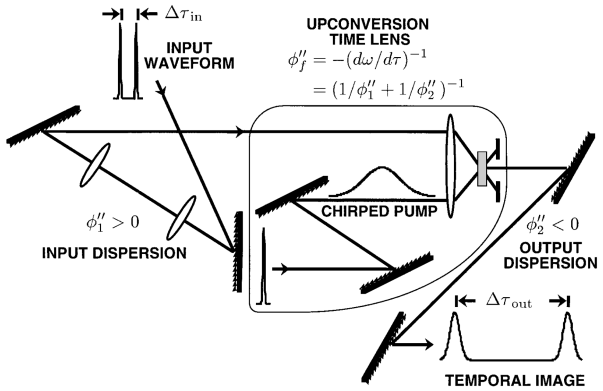

Fig. 2. Upconversion time microscope with positive magnification. The input and output dispersions are constructed with grating-pair dispersive delay lines. The time lens is produced by sum-frequency generation with a chirped optical pump pulse.

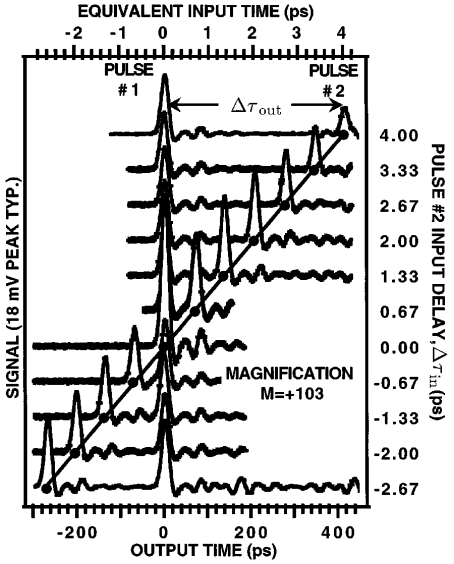

Fig. 3. Temporal images measured with 667-fs steps in the input delay of pulse #2, $\Delta\tau_{in}$. Each output delay, $\Delta\tau_{out}$, changed by 68.7 ps, indicating a magnification $M = +103$.

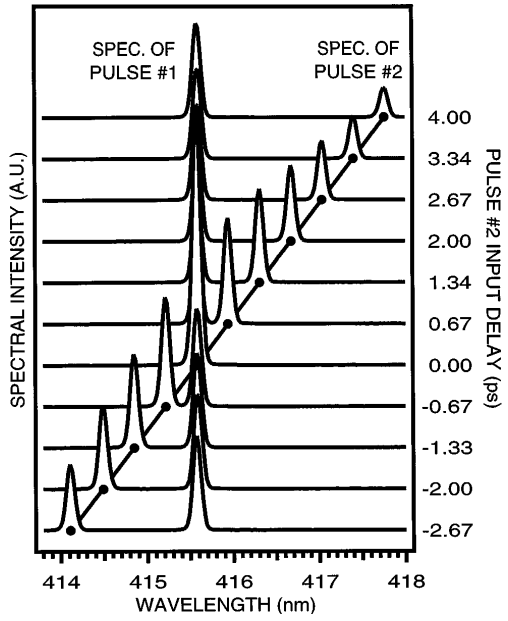

Fig. 4. Output spectra corresponding to the series of temporal images shown in Fig. 3. The frequency shift to delayed pulse #2 is the temporal analog of steering a beam with a lens by changing the beam's displacement from the lens axis.

efficiency but group-velocity mismatch between the fundamental and the upconverted signals is often unavoidable. This mismatch leads to an increase in the width of the system's impulse response and, more dramatically, to an additional source of roll-off in the field of view. Our system was configured to minimize the effects of these aberrations. The linear frequency shift with input delay and the symmetric form of the spectra in Fig. 4 suggest that our system is relatively free from these effects. The pulses recorded in the waveforms of Fig. 3 show that the photodiode (12.5 ps FWHM, with some ringing), and not aberrations in the imaging system itself, is the dominant distortion in the total measurement system. From a convolution of the ideal image, the ideal impulse response of the imaging system, and the measured impulse response of the photodiode, a 17.8-ps output pulse width was expected. The average measured width of pulse #2 in the images is 18.3 ps.

In conclusion, we have presented the fundamental principles and performance issues for a temporal imaging system and demonstrated a system with $+103\times$ magnification and 300-fs resolution. In addition, since the principles of temporal imaging do not rely on sampling, the system should be suitable for extending the range of single-shot waveform recorders such as optical streak cameras.

This work was supported in part by the U.S. Department of Energy's Lawrence Livermore National Laboratory under contract W-7405-Eng-48, the Lawrence Livermore National Laboratory Photonics Group under Laboratory Directed Research & Development grant 98-ERD-027, the National Science Foundation, the Advanced Thermionic Research Initiative program of the U.S. Air Force, and the David and Lucile Packard Foundation. C. V. Bennett's e-mail address is cvbennett@llnl.gov.

References

1. P. Tournois, J-L. Verner, and G. Bienvenu, C. R. Acad. Sci. (Paris) **267,** 375 (1968).
2. W. J. Caputi, IEEE Trans. Aerosp. Electron. Syst. **AES-7,** 269 (1971).
3. B. H. Kolner and M. Nazarathy, Opt. Lett. **14,** 630 (1989); erratum, **15,** 655 (1990).
4. B. H. Kolner, IEEE J. Quantum Electron. **30,** 1951 (1994).
5. P. Naulleau and E. Leith, Appl. Opt. **34,** 4119 (1995).
6. S. P. Dijaili, A. Dienes, and J. S. Smith, IEEE J. Quantum Electron. **26,** 1158 (1990).
7. J. A. Giormaine, M. A. Duguay, and J. W. Hansen, IEEE J. Quantum Electron. **QE-4,** 252 (1968).
8. D. R. Grischowsky, Appl. Phys. Lett. **26,** 566 (1974).
9. J. E. Bjorkholm, E. H. Turner, and D. B. Pearson, Appl. Phys. Lett. **26,** 564 (1975).
10. J. K. Wigmore and D. R. Grischowsky, IEEE J. Quantum Electron. **QE-14,** 310 (1978).
11. B. H. Kolner, Appl. Phys. Lett. **52,** 1122 (1988).
12. A. A. Godil, B. A. Auld, and D. M. Bloom, IEEE J. Quantum Electron. **30,** 827 (1994).
13. B. H. Kolner, C. V. Bennett, and R. P. Scott, Proc. SPIE **2116,** 245 (1994).
14. M. T. Kauffman, A. A. Godil, W. C. Banyai, and D. M. Bloom, Electron. Lett. **29,** 268 (1993).
15. M. T. Kauffman, W. C. Banyai, A. A. Godil, and D. M. Bloom, Appl. Phys. Lett. **64,** 270 (1994).
16. C. V. Bennett, R. P. Scott, and B. H. Kolner, Appl. Phys. Lett. **65,** 2513 (1994).
17. E. Arons, E. N. Leith, A. C. Tien, and R. Wagner, Appl. Opt. **36,** 2603 (1997).
18. E. B. Treacy, IEEE J. Quantum **QE-5,** 454 (1969).
19. B. H. Kolner, J. Opt. Soc. Am. A **11,** 3229 (1994).
20. O. E. Martinez, J. P. Gordon, and R. L. Fork, J. Opt. Soc. Am. A **1,** 1003 (1984).
21. J.-P. Foing, J.-P. Likforman, M. Joffre, and A. Migus, IEEE J. Quantum Electron. **28,** 2285 (1992).